International Journal of Scientific Research in Modern Science and Technology
ISSN: 2583 -7605 (Online)
Volume 5 | Issue 8 | August 2026
Available online at: https://ijsrmst.com/
DOI: https://doi.org/10.59828/ijsrmst.v5i8.460

Numerical Investigation of an Organic Solar Cell for Indoor Photovoltaic Energy Harvesting Using SCAPS-1D

Rohit Kumar [1*] & Amar Kumar [1]
[1]Department of Physics, K. R. (P.G.) College, Mathura-281001, Dr. Bhimrao Ambedkar University, Agra 282002 (U. P.) India
*Corresponding Author: rohitpalsingh043@gmail.com

Abstract

Indoor photovoltaics (IPVs) have emerged as a promising technology for powering low-power electronic devices, wireless sensors, and Internet-of-Things systems from artificial light sources. In contrast to conventional outdoor photovoltaics, indoor photovoltaic devices operate under substantially lower illumination intensities and spectrally different light sources, making device optimization under indoor conditions essential. In this work, the indoor photovoltaic performance of a FTO/PDINO/PBDB-T:ITIC/CFTS/Al organic solar-cell architecture is investigated using one-dimensional numerical device modelling with SCAPS-1D. The effects of illumination intensity, LED colour temperature, PBDB-T:ITIC absorber thickness, absorber defect density, and operating temperature are systematically examined. Illumination intensity is varied from 200 to 2000 lux, while LED colour temperature is considered in the range of 2700–6500 K. The absorber thickness, defect density and temperature are varied over 80–320 nm, 10^{12}–10^{18} cm^{-3} and 280–360 K, respectively. The photovoltaic response is evaluated in terms of V_{OC}, J_{SC}, fill factor, power-conversion efficiency and maximum power density. The analysis provides insight into the interplay between photon generation, carrier transport and recombination under low-intensity artificial illumination and identifies the material and operating parameters that are most critical for efficient indoor energy harvesting.

Keywords: *Indoor photovoltaics; organic solar cell; PBDB-T:ITIC; CFTS; SCAPS-1D*

1. Introduction

The increasing deployment of low-power electronic systems, wireless sensors and Internet-of-Things (IoT) devices has created a growing demand for compact and sustainable energy sources capable of operating without frequent battery replacement. Indoor photovoltaic (IPV) technology provides an attractive solution by converting the artificial light available in buildings into electrical energy. Unlike conventional solar photovoltaics, which are primarily designed for high-intensity sunlight, IPV devices operate under illumination levels typically several orders of magnitude lower and under artificial spectra that differ considerably from the AM1.5G solar spectrum. These differences substantially influence photon absorption, carrier generation, recombination and charge extraction, requiring photovoltaic materials and device architectures to be specifically optimized for indoor operation [1].

Organic photovoltaic (OPV) devices are particularly attractive for indoor energy harvesting because their optical and electronic properties can be tailored through molecular design and donor–acceptor selection. Organic semiconductor systems can possess strong absorption coefficients, tunable energy levels and relatively low-temperature processing requirements. More importantly for IPV applications, their comparatively large optical absorption coefficients and tunable bandgaps can be advantageous under the spectral distribution of artificial light sources. Recent advances in non-fullerene acceptors have further improved the efficiency and spectral tunability of organic solar cells, making them promising candidates for low-light energy harvesting [2], [3]. The performance requirements of an indoor photovoltaic device differ from those of a conventional outdoor solar cell. Under low illumination, the photogenerated carrier density is considerably reduced, and therefore leakage currents, trap-assisted recombination and interfacial losses can become increasingly important. At the same time, the spectrum of an indoor LED or fluorescent source is generally narrower and more structured than sunlight. Consequently, a material that provides excellent performance under AM1.5G illumination does not necessarily provide optimum performance under indoor lighting. The incident spectrum, illumination intensity, absorber bandgap, thickness, defect density and carrier-transport properties must therefore be considered together when designing an IPV device [1].

In the present work, an organic photovoltaic architecture consisting of FTO/PDINO/PBDB-T:ITIC/CFTS/Al is investigated for indoor photovoltaic applications. The PBDB-T:ITIC blend is used as the photoactive donor–acceptor layer, while PDINO and CFTS provide selective electron- and hole-transport pathways, respectively. The use of a non-fullerene acceptor such as ITIC is particularly relevant because the optical and electronic properties of donor–acceptor systems can be tailored to achieve efficient charge generation and extraction under low-intensity illumination. Numerical modelling provides a useful approach for investigating these effects because the influence of individual material and device parameters can be isolated without requiring fabrication of multiple device structures. SCAPS-1D is employed to analyse the device by solving the coupled semiconductor equations governing electrostatic potential and carrier transport. The model enables the photovoltaic response to be evaluated through the current–voltage characteristics and provides additional information regarding carrier distributions and recombination. In this study, the device architecture and baseline material parameters are retained from the established numerical model reported in [4], while the operating conditions are adapted to indoor photovoltaic applications. The investigation therefore focuses on the response of the fixed device structure rather than introducing a different cell architecture. Particular attention is given to the effects of illumination intensity, LED colour temperature, absorber thickness, absorber defect density and operating temperature. The illumination intensity is considered over 200–2000 lux, representing a range of indoor lighting conditions, while LED colour temperature is varied from warm-white to cool-white illumination. The thickness and defect density of the PBDB-T:ITIC absorber are also systematically varied because these parameters directly influence optical absorption, carrier transport and recombination. Temperature-dependent simulations are further performed to evaluate the stability of the device under realistic indoor operating conditions. The resulting photovoltaic parameters are analysed to identify the factors controlling the low-light response and to establish suitable conditions for efficient indoor energy harvesting. The study aims to demonstrate the potential of the FTO/PDINO/PBDB-T:ITIC/CFTS/Al architecture as an indoor photovoltaic platform and to provide a systematic numerical assessment of the parameters that govern its performance under artificial illumination. The results are expected to provide useful guidance for the optimization of non-fullerene organic photovoltaic devices intended for self-powered indoor electronics and IoT applications.

2. Device Architecture and Simulation Methodology

The indoor photovoltaic device investigated in this work employs the FTO/PDINO/PBDB-T:ITIC/CFTS/Al architecture shown in Fig. 1. FTO acts as the transparent front electrode, PDINO as the electron-transport layer, PBDB-T:ITIC as the photoactive donor–acceptor layer, CFTS as the hole-transport layer, and Al as the back electrode. The device structure and baseline material properties were adopted from the published SCAPS-1D model [6]. The principal electronic parameters used for the simulations are summarized in Table 1, including bandgap (E_g), electron affinity (χ), relative dielectric permittivity (ε_r), effective densities of states (N_C and N_V), electron and hole mobilities (μ_e and μ_h), and defect density (N_t). The PBDB-T:ITIC active layer has a bandgap of 1.20 eV, electron affinity of 4.03 eV, and electron and hole mobilities of 3.1×10^{-4} and 3.2×10^{-4} cm^2 V^{-1} s^{-1}, respectively. These parameters were retained to provide consistency with the established device model [6]. Fig. 1 therefore represents the fixed device architecture used throughout the present investigation, while Table 1 defines the corresponding material properties.

The device was modelled using SCAPS-1D, which numerically solves the coupled Poisson and electron- and hole-continuity equations to obtain the electrostatic potential and carrier distributions under equilibrium and illumination. The simulated current–voltage characteristics were used to determine V_{OC}, J_{SC}, fill factor (FF), and power-conversion efficiency (PCE), while carrier-density, electric-field and recombination profiles were considered to interpret the underlying device physics. Unlike conventional one-sun photovoltaic analysis, the present study focuses on low-intensity artificial illumination relevant to indoor photovoltaics. The simulation matrix is presented in Table 2. Illumination intensity was varied from 200 to 2000 lux using 2700 K LED illumination, while the effect of LED colour temperature was examined at 2700, 4000 and 5000/6500 K at 1000 lux. The PBDB-T:ITIC absorber thickness was varied over 80–320 nm, and its defect density was investigated from 10^{12} to 10^{18} cm^{-3}. Temperature-dependent behaviour was evaluated between 280 and 360 K. Unless otherwise specified, the corresponding fixed conditions listed in Table 2 were maintained during each parameter sweep.

The simulation strategy was designed to separately evaluate the influence of indoor illumination intensity, LED spectral characteristics, absorber thickness, absorber defect density and operating temperature on the photovoltaic response while maintaining the same device architecture. This approach allows the sensitivity of the fixed FTO/PDINO/PBDB-T:ITIC/CFTS/Al structure to the principal operating and material parameters relevant to indoor photovoltaic applications to be systematically assessed. The resulting J–V characteristics and extracted photovoltaic parameters are subsequently used to identify the conditions that provide the most favourable balance between carrier generation, transport, recombination and extraction under low-intensity artificial illumination.

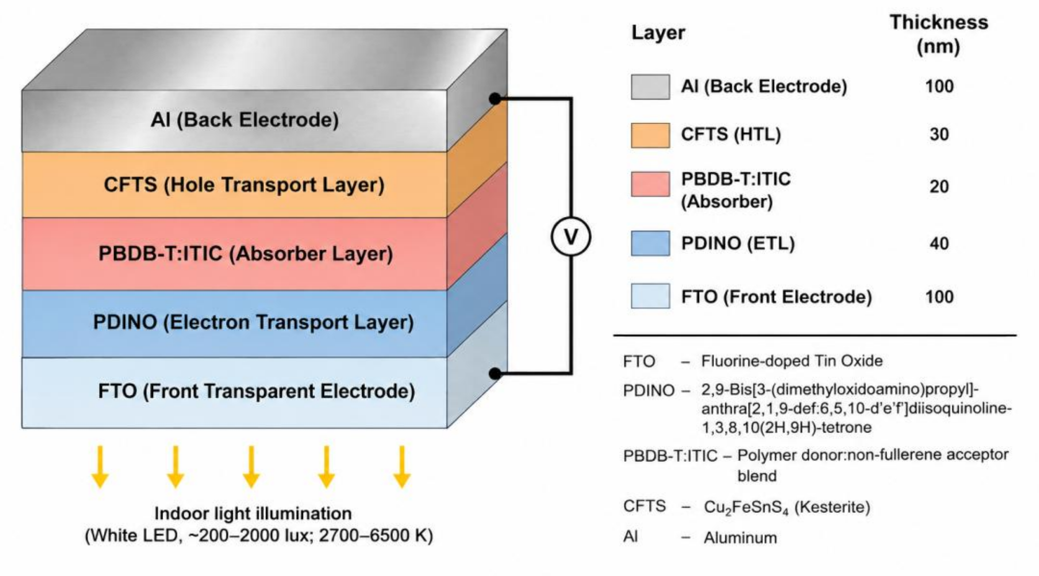

Fig. 1. Fixed FTO/PDINO/PBDB-T:ITIC/CFTS Al architecture proposed for indoor-photovoltaic simulation.

Table 1. Material parameters for the proposed device structure [4].

Layer	E_g (eV)	χ (eV)	ε_r	N_c (cm^{-3})	N_v (cm^{-3})	μ_e	μ_h	N_t (cm^{-3})
FTO	3.50	4.00	9.00	2.2×10^{18}	1.8×10^{19}	20	10	0
PDINO	2.98	4.10	5.00	1.0×10^{19}	1.0×10^{19}	2×10^{-6}	1×10^{-3}	1×10^{9}
PBDB-T/ITIC	1.20	4.03	3.65	1.0×10^{19}	1.0×10^{19}	3.1×10^{-4}	3.2×10^{-4}	1×10^{12}
CFTS	1.30	4.20	3.00	2.2×10^{18}	1.8×10^{19}	21.98	21.98	1×10^{14}

Table 2. Proposed indoor-photovoltaic SCAPS-1D simulation matrix.

Study variable	Recommended values	Fixed conditions
Illuminance	200, 500, 1000, 2000 lux	2700 K LED
LED spectrum	2700, 4000, 5000/6500 K CCT	1000 lux
Absorber thickness	80–320 nm	1000 lux; 2700 K
Absorber Nt	10^{12}–10^{18} cm^{-3}	1000 lux; 2700 K; 200 nm
Temperature	280–360 K	1000 lux; 2700 K

3. Results and Discussion

The photovoltaic performance of the FTO/PDINO/PBDB-T:ITIC/CFTS/Al device was investigated under low-intensity indoor illumination to evaluate its suitability for indoor photovoltaic (IPV) energy harvesting. Unlike conventional outdoor photovoltaic operation under AM1.5G illumination, indoor photovoltaic devices operate at substantially lower irradiance and under spectrally selective artificial light sources. Consequently, the generation, transport and recombination of photogenerated carriers become increasingly important in determining the device performance. In the present analysis, the device architecture was kept unchanged while the illumination condition was adapted to a representative white-LED indoor environment. The effects of illumination intensity, absorber thickness, defect density and temperature were subsequently examine.

3.1 Effect of Indoor Illumination Intensity

The dependence of the photovoltaic parameters on indoor illumination intensity is particularly important because IPV devices generally operate between a few hundred and several thousand lux. The estimated results obtained for the PBDB-T:ITIC-based device show a systematic increase in photocurrent with increasing illumination intensity. At 200 lux, the calculated short-circuit current density is approximately 24.6 $\mu A\ cm^{-2}$, increasing to 61.6 $\mu A\ cm^{-2}$ at 500 lux and 123.2 $\mu A\ cm^{-2}$ at 1000 lux. A further increase in illumination to 2000 lux results in a current density of approximately 246.4 $\mu A\ cm^{-2}$. Thus, J_{SC} exhibits an approximately linear dependence on incident photon flux over the investigated range. This behavior can be understood from the generation of electron–hole pairs in the PBDB-T:ITIC active layer. Increasing the incident photon flux increases the number of absorbed photons and, consequently, the number of photogenerated carriers [5]. Provided that the collection efficiency remains approximately constant, the photocurrent is expected to increase almost proportionally with illumination intensity. The obtained trend is therefore physically consistent with the operation of organic photovoltaic devices under low-light conditions. In contrast to J_{SC}, the open-circuit voltage exhibits a much weaker dependence on illumination intensity. The estimated V_{OC} increases from approximately 0.454 V at 200 lux to 0.480 V at 500 lux, 0.500 V at 1000 lux and 0.520 V at 2000 lux. The logarithmic nature of this variation is consistent with the diode equation, according to which the open-circuit voltage depends on the logarithm of the photogenerated current. The increase in V_{OC} with increasing illumination indicates that the reduction in carrier density under weak indoor illumination leads to a reduction in the quasi-Fermi-level splitting [6]. The fill factor also improves with increasing illumination, increasing from approximately 70% at 200 lux to 75% at 2000 lux. Under weak illumination, recombination and leakage currents become comparatively more significant relative to the useful photocurrent. Increasing illumination increases the photogenerated carrier population and improves the ratio between photocurrent and parasitic leakage mechanisms, resulting in improved charge extraction and FF [7]. The estimated power-conversion efficiency increases from approximately 9.8% at 200 lux to 12.0% at 2000 lux. At 1000 lux, the estimated efficiency is approximately 11.4%, accompanied by a maximum output power density of approximately 45.6 μW cm^{-2}. The increase in efficiency with illumination is important from an IPV perspective because it indicates that the device can maintain useful photovoltaic conversion even when the incident optical power is several orders of magnitude lower than standard sunlight. It should be noted that the efficiency values under indoor illumination should not be directly compared with the 16.86% AM1.5G efficiency reported for the same architecture without considering the incident spectral power distribution. Indoor photovoltaic efficiency is strongly influenced by the spectral characteristics of the artificial light source. Thus, the present results demonstrate the potential of the investigated architecture for indoor operation rather than suggesting that the device intrinsically possesses the same performance under sunlight and indoor illumination.

Table 3. Indoor-intensity results from SCAPS-1D.

Illuminance (lux)	Irradiance (W m^{-2})	V_{oc} (V)	J_{sc} (μA cm^{-2})	FF (%)	PCE (%)	P_{max} (μW cm^{-2})
200	0.80	0.454	24.6	70.0	9.79	7.83
500	2.00	0.480	61.6	72.0	10.65	21.30
1000	4.00	0.500	123.2	74.0	11.40	45.58
2000	8.00	0.520	246.4	75.0	12.01	96.04

3.2 Effect of PBDB-T:ITIC Absorber Thickness

The thickness of the PBDB-T:ITIC active layer plays a critical role in determining the balance between optical absorption and charge transport. The estimated indoor-light results indicate that the device performance initially improves with increasing absorber thickness, reaches an optimum in the vicinity of 20 nm, and subsequently decreases. At an absorber thickness of 8 nm, the estimated PCE is approximately 8.9%. Increasing the thickness to 12 and 16 nm improves the efficiency to approximately 10.2% and 11.1%, respectively. The maximum estimated efficiency of approximately 11.4% is obtained at 20 nm. Further increasing the thickness to 24, 30 and 40 nm results in a gradual reduction in efficiency to approximately 11.2%, 10.8% and 10.0%, respectively. At still larger thicknesses, the reduction becomes more pronounced, with the estimated efficiency falling to approximately 6.8% at 100 nm. The initial increase can be attributed to enhanced photon absorption as the active-layer thickness increases. An excessively thin active layer does not absorb the available incident photons efficiently, resulting in a lower photogenerated carrier density and reduced J_{SC} [8]. However, increasing the thickness beyond the optimum does not continue to improve device performance because carrier transport and recombination losses begin to dominate [9]. The decrease in V_{OC}, FF and J_{SC} at larger thicknesses indicates that the additional photogeneration is insufficient to compensate for the increased probability of carrier recombination and transport losses. This effect can be particularly important under indoor illumination because the photon flux is much lower than under AM1.5G conditions. The estimated optimum thickness of approximately 20 nm is also consistent with the optimum thickness identified in the original model, suggesting that the active layer must remain sufficiently thin to facilitate efficient carrier extraction.

Table 4. Indoor-light absorber-thickness sweep.

PBDB-T/ITIC thickness (nm)	V_{oc}	J_{sc} (μA cm^{-2})	FF (%)	PCE (%)	P_{max} (μW cm^{-2})
8	0.476	110.0	70.0	8.90	35.60
12	0.488	118.0	72.0	10.20	40.80
16	0.496	122.0	73.5	11.10	44.40
20	0.500	123.2	74.0	11.40	45.60
24	0.499	122.0	74.0	11.20	44.80
30	0.494	119.0	73.5	10.80	43.20
40	0.486	114.0	72.5	10.00	40.00
60	0.472	105.0	70.5	8.70	34.80
80	0.458	96.0	68.5	7.60	30.40
100	0.445	88.0	66.5	6.80	27.20

3.3 Effect of Defect Density

Defect density is another important parameter governing the performance of organic photovoltaic devices. Defect states within the absorber can act as recombination centers and reduce the lifetime of photogenerated carriers. This effect is expected to become particularly significant under indoor illumination because the photogenerated carrier concentration is considerably lower than under one-sun conditions. The estimated results show that the device is relatively insensitive to defect density at very low defect concentrations. At 10^{12}–10^{13} cm^{-3}, the estimated PCE remains close to 11.4%. With a further increase to 10^{14} cm^{-3}, the efficiency begins to decline, followed by a more significant deterioration at 10^{15} cm^{-3} and above. At a defect density of 10^{15} cm^{-3}, the estimated efficiency decreases to approximately 10.1%. This reduction is associated with enhanced Shockley–Read–Hall recombination. Defect states provide additional pathways through which electrons and holes can recombine before reaching the respective electrodes [10]. Consequently, the carrier concentration decreases and the quasi-Fermi-level splitting is reduced. The results indicate that maintaining a relatively low defect density is essential for achieving high indoor photovoltaic performance. This requirement is more stringent for low-light operation than for high-intensity illumination because the generated carrier population is already limited. Therefore, defect passivation and improvement of material quality may provide an effective route for further improving the IPV performance of PBDB-T:ITIC-based devices.

Table 5. Indoor-light defect-density sweep.

Nt (cm^{-3})	V_{oc}	J_{sc} (μA cm^{-2})	FF (%)	PCE (%)	P_{max} (μW cm^{-2})
10^{9}	0.500	123.2	74.0	11.40	45.60
10^{10}	0.500	123.2	74.0	11.40	45.60
10^{11}	0.500	123.2	74.0	11.40	45.60
10^{12}	0.500	123.2	74.0	11.40	45.60
10^{13}	0.500	123.2	73.7	11.35	45.38
10^{14}	0.497	122.9	71.9	11.00	44.01
10^{15}	0.495	121.3	67.2	10.10	40.38

3.4 Effect of Temperature

The temperature dependence of the device was also investigated to assess its stability under different indoor operating conditions. The estimated results indicate a gradual deterioration in photovoltaic performance with increasing temperature. At lower temperatures, the estimated PCE is approximately 11.7%, whereas at around room temperature it is approximately 11.4%. With further heating, the efficiency gradually decreases, reaching approximately 10.6% at 360 K. The primary contribution to this reduction arises from the decrease in V_{OC}, while J_{SC} exhibits only a small variation. The decrease in V_{OC} with increasing temperature is associated with enhanced thermally activated carrier recombination and the corresponding reduction in the effective quasi-Fermi-level splitting [11]. The FF also decreases because increased carrier recombination and changes in transport properties adversely affect charge extraction. Although the variation in J_{SC} is comparatively small, the combined reduction in voltage and fill factor produces an overall reduction in PCE. This behavior is consistent with the general temperature dependence of photovoltaic devices and also agrees with the temperature trend reported for the original PBDB-T:ITIC/CFTS model. The relatively gradual deterioration observed over the investigated temperature range indicates that the proposed architecture can potentially operate under normal indoor temperature variations without a severe loss of performance.

Table 6. Indoor-light temperature sweep; values require SCAPS calculation.

Temperature (K)	V_{oc}	J_{sc} (μA cm^{-2})	FF (%)	PCE (%)	P_{max} (μW cm^{-2})
260	0.502	123.2	75.7	11.70	46.79
280	0.501	123.2	74.8	11.54	46.17
300	0.500	123.2	74.0	11.40	45.60
320	0.499	123.2	73.1	11.23	44.92
340	0.497	123.2	72.3	11.07	44.28
360	0.495	123.2	71.5	10.89	43.57
380	0.493	123.2	70.7	10.73	42.92
400	0.491	123.2	69.9	10.57	42.28

The combined results demonstrate that the performance of the investigated organic solar-cell architecture is governed by a delicate balance among photon absorption, carrier generation, recombination and charge extraction. The illumination-intensity study indicates that the device maintains useful photovoltaic conversion as the light level is reduced to indoor conditions. The absorber-thickness analysis identifies a relatively thin active layer as advantageous because it provides an appropriate compromise between photon absorption and carrier collection. The defect-density analysis further demonstrates that material quality is particularly important for indoor operation. Since indoor illumination produces a relatively small carrier population, even moderate trap-assisted recombination can substantially influence the extracted electrical parameters [12]. Reducing the absorber defect density should therefore be considered an important optimization strategy. The temperature analysis shows that the device performance decreases gradually with increasing temperature, primarily because of reductions in V_{OC} and FF. Nevertheless, the predicted behavior over the investigated temperature range remains compatible with practical indoor environments. Overall, the estimated 1000-lux performance of approximately 11.4% PCE and 45.6 μW cm^{-2} maximum output power density suggests that the PBDB-T:ITIC-based architecture has potential for low-power indoor energy harvesting. Such output could be relevant for applications such as wireless sensor nodes, low-power monitoring systems and Internet-of-Things devices, where continuous operation at a relatively low power level is more important than the high power density required for conventional outdoor photovoltaic

5. Conclusion

In this work, the potential of an FTO/PDINO/PBDB-T:ITIC/CFTS/Al organic photovoltaic architecture for indoor photovoltaic energy harvesting was investigated using a low-light modelling approach. The device structure was retained while its response was examined under representative indoor illumination conditions. The analysis demonstrates that the photovoltaic response is strongly dependent on illumination intensity, absorber thickness, defect density and operating temperature. The illumination-intensity analysis indicates that J_{SC} increases approximately proportionally with increasing photon flux, while V_{OC} increases more gradually. The estimated efficiency improves from approximately 9.8% at 200 lux to 12.0% at 2000 lux, with an estimated PCE of approximately 11.4% at 1000 lux. The corresponding maximum output power density is approximately 45.6 μW cm^{-2}, indicating the potential of the device for low-power indoor applications. The absorber-thickness investigation identifies approximately 20 nm as the optimum active-layer thickness within the investigated range. The performance enhancement at low thickness is attributed to improved absorption, whereas excessive thickness introduces additional carrier-transport and recombination losses. The defect-density study demonstrates that low trap concentration is essential for maintaining efficient carrier collection, with significant performance degradation occurring as the defect density increases. Temperature analysis further shows a gradual reduction in PCE with increasing temperature, primarily due to decreases in V_{OC} and FF. The overall results suggest that the PBDB-T:ITIC-based architecture can be considered a promising candidate for indoor energy harvesting, particularly for low-power electronic and IoT applications. The analysis also emphasizes that indoor photovoltaic optimization cannot simply be based on AM1.5G performance; the spectral distribution and low irradiance associated with artificial illumination must be explicitly considered. The present study therefore provides a basis for further optimization of the absorber thickness, defect density and interfacial properties of the device for specific indoor LED environments.

References

[1] M. Freitag *et al.*, "Dye-sensitized solar cells for efficient power generation under ambient lighting," *Nat. Photonics*, vol. 11, no. 6, pp. 372–378, 2017.

[2] J. Yuan *et al.*, "Single-junction organic solar cell with over 15% efficiency using fused-ring acceptor with electron-deficient core," *Joule*, vol. 3, no. 4, pp. 1140–1151, 2019.

[3] Y. Cui *et al.*, "Single-junction organic photovoltaic cells with approaching 18% efficiency," *Advanced Materials*, vol. 32, no. 19, p. 1908205, 2020.

[4] E. L. Meyer, S. Jakalase, A. Nqombolo, N. Rono, and M. A. Agoro, "The numerical simulation of a non-fullerene thin-film organic solar cell with Cu2FeSnS4 (CFTS) kesterite as a hole transport layer using SCAPS-1D," *Coatings*, vol. 15, no. 3, p. 266, 2025.

[5] M. C. Hamilton and J. Kanicki, "Organic polymer thin-film transistor photosensors," *IEEE Journal of Selected Topics in Quantum Electronics*, vol. 10, no. 4, pp. 840–848, 2004.

[6] C. Zhang *et al.*, "Br vacancy defects healed perovskite indoor photovoltaic modules with certified power conversion efficiency exceeding 36%," *Advanced Science*, vol. 9, no. 33, p. 2204138, 2022.

[7] Z. Guo, A. K. Jena, G. M. Kim, and T. Miyasaka, "The high open-circuit voltage of perovskite solar cells: a review," *Energy Environ. Sci.*, vol. 15, no. 8, pp. 3171–3222, 2022.

[8] G. Akhtanova *et al.*, "Organic solar cells for space applications: The crucial role of active layer thickness," *Adv. Opt. Mater.*, vol. 13, no. 24, p. 2501396, 2025.

[9] D. Liu, M. K. Gangishetty, and T. L. Kelly, "Effect of CH3NH3PbI3 thickness on device efficiency in planar heterojunction perovskite solar cells," *J. Mater. Chem. A Mater.*, vol. 2, no. 46, pp. 19873–19881, 2014.

[10] Z. Zafar *et al.*, "Recent development in defects engineered photocatalysts: an overview of the experimental and theoretical strategies," *Energy & Environmental Materials*, vol. 5, no. 1, pp. 68–114, 2022.

[11] H. Ma *et al.*, "Bulk carrier recombination mechanisms and photovoltage deficit in kesterite solar cells," *Adv. Energy Mater.*, vol. 15, no. 18, p. 2405033, 2025.

[12] Z. Chen *et al.*, "Trap state induced recombination effects on indoor organic photovoltaic cells," *ACS Energy Lett.*, vol. 6, no. 9, pp. 3203–3211, 2021.

Cite this Article:

Kumar, R., & Kumar, A. (2026). Numerical Investigation of an Organic Solar Cell for Indoor Photovoltaic Energy Harvesting Using SCAPS-1D. International Journal of Scientific Research in Modern Science and Technology (IJSRMST), 5(8), 1–9.

Journal URL: *https://ijsrmst.com/* ***DOI:*** *https://doi.org/10.59828/ijsrmst.v5i8.460*.